

StrideNET: Swin Transformer for Terrain Recognition with Dynamic Roughness Extraction

Maitreya Shelare¹, Neha Shigvan², Atharva Satam³, Poonam Sonar⁴

Abstract—Advancements in deep learning are revolutionizing the classification of remote-sensing images. Transformer-based architectures, utilizing self-attention mechanisms, have emerged as alternatives to conventional convolution methods, enabling the capture of long-range dependencies along with global relationships in the image. Motivated by these advancements, this paper presents StrideNET, a novel dual-branch architecture designed for terrain recognition and implicit properties estimation. The terrain recognition branch utilizes the Swin Transformer, leveraging its hierarchical representation and low computational cost to efficiently capture both local and global features. The terrain properties branch focuses on the extraction of surface properties such as roughness and slipperiness using a statistical texture analysis method. By computing surface terrain properties, an enhanced environmental perception can be obtained. The StrideNET model is trained on a dataset comprising four target terrain classes: Grassy, Marshy, Sandy, and Rocky. StrideNET attains competitive performance compared to contemporary methods. The implications of this work extend to various applications, including environmental monitoring, land use and land cover (LULC) classification, disaster response, precision agriculture, and much more.

Index Terms—Swin Transformer, Deep Learning, Terrain Partition, Land Surface Roughness, Remote Sensing

I. INTRODUCTION

TERRAIN recognition and extraction of its properties such as roughness & slipperiness, through the integration of deep learning and remote sensing techniques, offer substantial benefits across various domains. These applications extend to land use and land cover (LULC) classification [1], ecological monitoring [2], geographical mapping [3], natural feature detection [4], and disaster management [5].

Traditionally, terrain recognition was done manually by experts, which was time-consuming and expensive. Thus, to automate this process, various image processing techniques were proposed [6]. However, they failed to classify rapidly changing landscapes accurately. This drawback was overcome by using deep learning techniques.

The Convolutional Neural Network (CNN) stands as one of the most extensively employed deep learning methodologies. CNN based methods excel at classifying images with high accuracy even in very challenging situations [7]–[9]. However, their locality bias [10] limits them from capturing long-range dependencies and global relationships across the image. Also, they lack the ability to explain the rationale behind their predictions [11].

These limitations of CNN-based methods are overcome by the vision transformer [12] and its variants [13], [14], which have shown promising results in various computer vision tasks.

Thus, this paper proposes a novel dual branch transformer-based network called StrideNET: Swin Transformer for Terrain Recognition with Dynamic Roughness Extraction.

The terrain recognition branch utilizes the Swin Transformer to classify different terrains, while the terrain properties branch focuses on the extraction of surface properties such as roughness and slipperiness using a statistical texture analysis method.

Swin (Shifted Window) is a variant of vision transformer that constructs a hierarchical representations of input image data. The shifted window-based self-attention of the Swin transformer produces cross-window connections by limiting the non-overlapping local window computations. Moreover, it exhibits linear computational complexity relative to the size of the input image. These characteristics make it computationally efficient for computer vision tasks, including image classification [14].

Swin Transformer provide computational efficiency with a time complexity of $O(mn)$ for high-resolution data than the complexity of $O(n^2)$ of traditional vision transformer, for reasonably small window size m [14]. Moreover, it offers higher generalization capabilities over CNNs by considering the relationship between different features of an image [15].

For terrain roughness extraction, a statistical variance-based texture analysis method was utilized. Texture feature analysis determines how pixels interact within local areas of an image by capturing changes in grayscale levels. It uses statistical methods to model texture as a random field and fits a probability distribution to the intensity distribution within that texture [16]. The variance of each patch was calculated of the of subdivided input image and then corresponding roughness factor was estimated.

The study’s key contributions are summarized below:

- 1) A novel technique for extraction terrain properties such as roughness and slipperiness is proposed, which utilize a statistical variance-based texture analysis algorithm.
- 2) The StrideNET network demonstrates state of the art performance in terrain classification task, showcasing the efficacy of the proposed network.

The following is the structure of the subsequent sections of this paper. The overview of existing work in terrain classification and roughness estimation is given in Section II. The proposed approach is elaborated in Section III. Section IV explores the analysis and discussion of the experimental results. Finally, Section V provides a summary of this work.

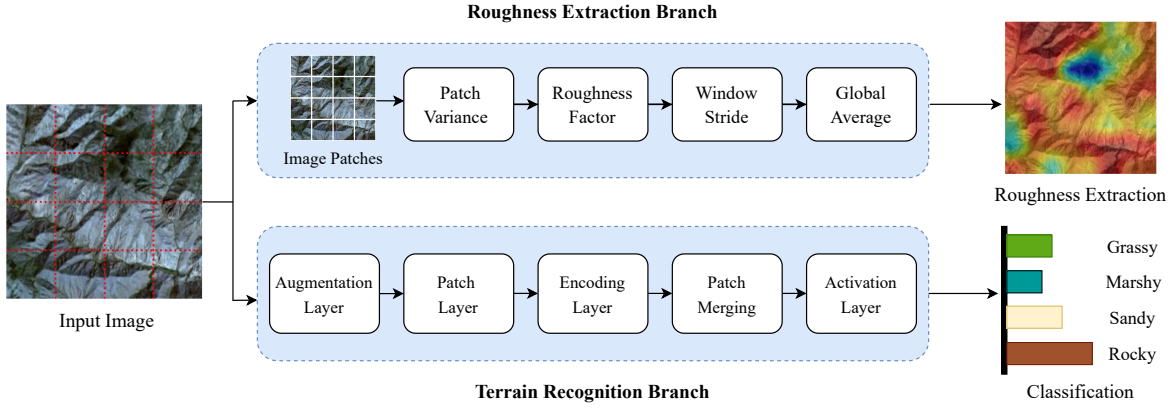


Fig. 1. StrideNET Architecture

II. RELATED WORKS

This section explores related works for terrain recognition and roughness extraction of remote sensing images.

A. Terrain Recognition

The Faster-RCNN model [17], employing a deep convolutional neural network (DCNN), region proposal network (RPN), and object detection network (ODN), achieves accurate detection of closely spaced craters in aerial and remote sensing imagery for crater identification. However, it is limited to only binary classification and cannot classify multiple terrain features simultaneously.

A novel Object Detection Network (ODN) introduced in [18] aims to identify various natural terrain features like craters, volcanoes, and hills. This work compares the performance of four Convolutional Neural Network (CNN) models: ZF-Net [19], Inception-ResNet [20], VGG-16 [21], and DenseNet 121 [22]. Inception-ResNet demonstrates the best accuracy amongst the models.

In [23], a comparative analysis of terrain classification is conducted, evaluating texture, color, and convolutional features alongside classifiers like support vector machines and K-nearest neighbors. The study proposes a lightweight Convolutional Neural Network architecture that achieves competitive results in classifying six terrain classes from a subset of the DeepSat SAT-6 dataset [24]. Notably, convolutional features demonstrate the highest accuracy, surpassing both color and texture features.

In [25], the emphasis is placed on the effectiveness of integrating the AlexNet model for feature extraction with K-nearest neighbors (KNN) for classification. This integration enhances the efficiency and accuracy of remote sensing image classification tasks. The proposed methodology demonstrated noteworthy outcomes across three datasets: AID [26], NWPU-RESISC45 [27], and UC Merced Land Use [28].

In [29], the effectiveness of different transformer-based models is surveyed for remote sensing tasks. The study

outlines how vision transformers can effectively capture long-range dependencies and emphasizes their flexibility in representation, leading to superior performance.

In [30], a novel Remote-Sensing Transformer (TRS) for scene classification is proposed, integrating CNN with transformers. The model replaces spatial convolutions with Multi-Head Self-Attention, leading to enhanced performance in remote-sensing tasks.

In [31], the efficacy of vision transformers with the attention mechanism is emphasized over standard CNNs. Likewise, [32] introduces vision transformers for scene classification, utilizing self-attention mechanism to capture contextual relations among image pixels. The study also explores the capabilities of data-efficient image transformer (DeiT) [13], trained via knowledge distillation with reduced data.

The ViT-CL model [33] integrates Vision Transformer (ViT) with supervised contrastive learning (CL) for scene classification. Utilizing a joint loss function that integrates cross-entropy loss and supervised contrastive loss, the model enhances robustness and discriminative feature learning. Experimental results illustrate the effectiveness of vision transformers over CNNs in the classification of remote sensing imagery.

In [34], the Swin Transformer algorithm was proposed for classifying complex coastal wetlands in Saint John City, Canada. Comparative analysis with AlexNet and VGG-16, two CNN classifiers, demonstrated superior accuracy and F1 scores of the Swin Transformer across diverse wetland types, surpassing CNNs notably.

In [35], a novel multi-model network is presented, which integrates transformers with Convolutional Neural Networks, incorporating VGG-16, 3D CNN, and Swin Transformer models. The ensemble model exhibited substantial performance improvements in terms of average accuracy and F-1 scores across various wetland types in comparison to individual classifiers such as random forests and support vector machines (SVM).

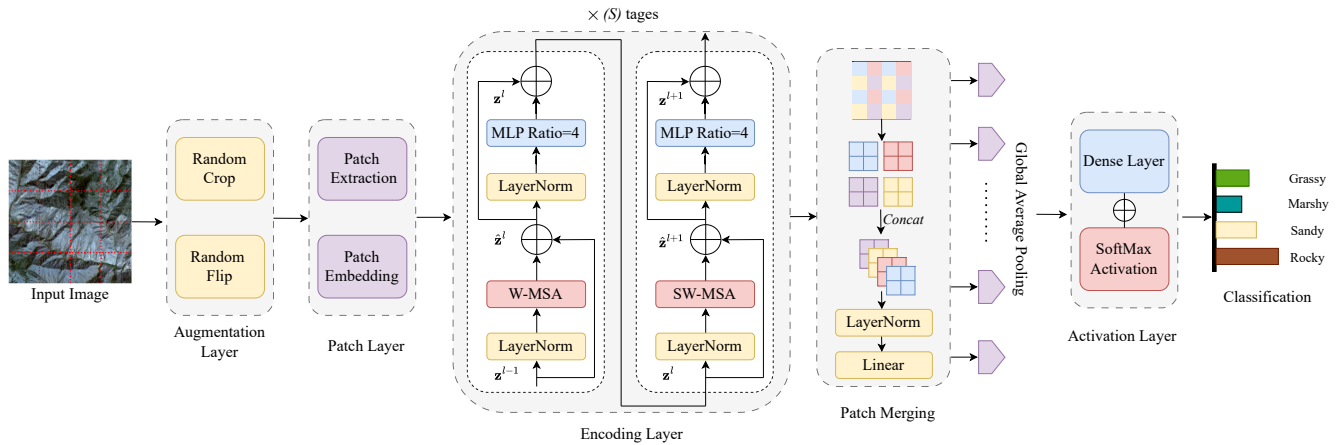


Fig. 2. Classification branch

B. Terrain Roughness

In [36], a method to predict pixel-wise labels of terrains such as stone, sand, grass, etc. is proposed, along with roughness estimation, using a deep neural network. Terrain segmentation is done using the SegNet [37] and ERFNet [38] architectures. A model previously trained on the Cityscapes dataset [39] is utilized for faster training and generalization. For roughness estimation, the primitive appearance features from the lower layers of CNN are extracted, and up-projection blocks [40] are employed to recover the spatial resolution of downsampled feature representations.

In [41], a tapered whisker with multiple sensors is employed to capture vibrations and perform terrain classification at low computational cost. The whiskered robot utilizes a self-supervised learning method through reservoir computing. Additionally, it can estimate terrain properties such as roughness at different speeds.

III. METHODOLOGY

This section presents the proposed StrideNET network, and outlines its network components for terrain recognition and roughness extraction.

The StrideNET architecture is explained in Section III-A, and its two constituent branches, Terrain Recognition and Roughness Extraction, are discussed in sections III-B and III-C respectively.

A. StrideNET Architecture

The StrideNET architecture is presented in Fig. 1. The input image is passed through two branches, one for terrain recognition and other for roughness extraction.

In classification branch, as shown in Fig. 2, different image augmentation operations are performed on the image to ensure model robustness. Then, the image undergoes a patch extraction process where it is divided into non-overlapping patches representing local regions.

Then positional embedding is performed for encoding spatial information of the patches to assist in capturing spatial

relationships between different patches. The input patches, along with their corresponding positional embedding, are then passed to the encoding layer of the Swin Transformer.

The encoding layers are comprised of successive transformer blocks having multiple attention heads and a feedforward neural network. The windowed self-attention mechanism of Swin transformer is used to efficiently capture long-range dependencies within the image. The output of this is then applied to a feedforward neural network to perform feature transformation.

Thereafter, patch merging is performed to downsample feature maps between each stage of the transformer, varying the last stage. Then global average pooling is done to compress the spatial information from the feature maps into a fixed-length vector, to ensure uniformity of the input size.

The output of the global average pooling layer is then fed into the dense layer, which maps the high-dimensional feature representation to the desired output dimensions, corresponding to the number of classes. Finally, the Softmax activation function assigns probabilities to the classes, resulting in accurate terrain recognition.

In the roughness extraction branch, a statistical texture analysis method is utilized, given by algorithm 2. First, the image is divided into disjoint patches, and then the variance of each patch is calculated using Eq. 5. Then, the roughness factor is computed, using Eq. 6.

Thereafter, window shifting and global averaging techniques are used to capture both local and global characteristics of texture. Window shifting provides a detailed analysis of local features, while global averaging computes overall roughness across the entire image.

To visualize the roughness property functions such as resize and normalize are implemented on the obtained data. The various roughness levels present are then visualized. Finally, the obtained roughness values are visualized as an overlay over the original image.

B. Terrain Recognition Branch

The Swin Transformer constructs a hierarchical representation of image features and exhibits linear computational complexity for . It has achieved excellent performance in different computer vision applications, such as image classification, object detection, etc. [14].

The Swin Transformer differs from traditional Transformers in several ways. First, it employs a hierarchical structure enabling efficient processing of high-resolution images. Second, it adopts a shifted windowing approach that confines self-attention to disjoint windows, while allowing cross-window connectivity. Third, it uses relative positional bias to enhance the model’s performance.

1) *Self-attention in non-overlapped windows*: Non-overlapping window self-attention is a method used to apply self-attention to high-resolution images without incurring the computational overhead of global self-attention. This technique partitions the image into disjoint windows & applies self-attention in each window.

Shifted window self-attention further improves the capacity of the model to capture long-range dependencies by introducing cross-window connections. Multi-head self attention (*MSA*) is a self-attention mechanism that is utilized to learn long-range dependencies among pixels in an image. The formula for *MSA* takes three inputs:

$$\Omega(\mathcal{MSA}) = 4hwC^2 + 2(hw)^2C \quad (1)$$

Windowed multi-head self-attention ($\mathcal{W} - \mathcal{MSA}$) block in the Swin Transformer, is a variant of *MSA* that is more efficient to compute. The formula for $\mathcal{W} - \mathcal{MSA}$ takes four inputs:

$$\Omega(\mathcal{W} - \mathcal{MSA}) = 4hwC^2 + 2(M)^2hwC \quad (2)$$

where h and w represent the height & width of feature maps. C denotes the number of channels in the input feature map, and M is the number of attention heads.

2) *Shifted window partition in successive blocks*: Shifted window partitioning improves the Swin Transformer’s capability to capture long-range dependencies by alternating between two partitioning configurations across consecutive blocks. This technique introduces cross-window connections, enabling the model to attend to tokens in other windows and effectively capture global context.

$$\begin{aligned} \hat{\mathbf{z}}^l &= \mathcal{W} - \mathcal{MSA}(\mathcal{LN}(\mathbf{z}^{l-1})) + \mathbf{z}^{l-1}, \\ \mathbf{z}^l &= \mathcal{MLP}(\mathcal{LN}(\hat{\mathbf{z}}^l)) + \hat{\mathbf{z}}^l, \\ \hat{\mathbf{z}}^{l+1} &= \mathcal{SW} - \mathcal{MSA}(\mathcal{LN}(\mathbf{z}^l)) + \mathbf{z}^l, \\ \mathbf{z}^{l+1} &= \mathcal{MLP}(\mathcal{LN}(\hat{\mathbf{z}}^{l+1})) + \hat{\mathbf{z}}^{l+1}, \end{aligned} \quad (3)$$

$\mathcal{W} - \mathcal{MSA}(\cdot)$ operation applies self-attention within local windows, dividing the input feature map into disjoint windows.

$\mathcal{LN}(\cdot)$ is a normalization technique applied to the output of each layer. The $\mathcal{MLP}(\cdot)$ comprises 2 fully connected layers, each equipped with a GELU activation function in between $\mathcal{SW} - \mathcal{MSA}(\cdot)$. The variable \mathbf{z} represents the feature map at each stage of the Swin Transformer.

3) *Relative position bias*: It refers to the way that the attention mechanism learns to attend to various segments of the input sequence based on their relative positions.

$$\text{Attention}(Q, K, V) = \text{SoftMax}(QK^T/\sqrt{d} + B)V \quad (4)$$

where Q , K and V are the query, key and value vectors respectively. B is the relative position bias matrix & d denotes the dimension of the key vector.

The relative position bias matrix B is a learned matrix that contains information about the relative positions of the elements in the input sequence. It improves the performance of attention mechanisms on a variety of tasks because it allows the attention mechanism to learn more effective ways of attending to the input sequence.

Algorithm 1 Swin Transformer for Terrain Recognition

- 1: **Input:**
Image: $I \in \mathbb{R}^{224 \times 224 \times 3}$
 - 2: **Parameters:**
Patch size: $P = 4 \times 4$
Embedded Dimension: $D = 96$
Heads in MSA: H
Transformer Blocks: $T = \{2, 2, 6, 2\}$
 - 3: **Initial Embeddings:**
Split I into patches: $I_p \in \mathbb{R}^{56 \times 56 \times 48}$
Embed: $E_1 = \text{Linear}(I_p); E_1 \in \mathbb{R}^{56 \times 56 \times D}$
 - 4: **for** $s = 2$ to 4 **do**
 - 5: **a. Patch Merge:**
 - 6: $E_s = \text{Merge}(E_{s-1})$
 - 7: **b. Process:**
 - 8: **for** $t = 1$ to $T[s]$ **do**
 - 9: $E_s = \text{TransformerBlock}(E_s)$
 - 10: **end for**
 - 11: **end for**
 - 12: **Global Average Pooling:**
 $V = \text{GAP}(E_4); V \in \mathbb{R}^D$
 - 13: **Classifier:**
 $O = \text{Softmax}(\text{Linear}(V))$
 - 14: **Output:**
 O : Class Probabilities of Different Terrains
-

Algorithm 1 represents terrain recognition using a SWIN transformer. The process commences by splitting an image (I) into patches of size P (4×4). This creates a new 3D tensor Ip of size $56 \times 56 \times 48$, where each element represents a patch in the image. Then a linear transformation (E) is applied to each patch to embed it into a D-dimensional vector, creating a new 3D tensor E of size $56 \times 56 \times 96$.

Thereafter, the image is processed through four stages where smaller patches are merged into larger ones. Subsequently, the merged patches are subjected to transformer blocks. A set of Transformer blocks are applied sequentially. These blocks consist of Multi-Scale Self-Attention for focusing informative parts of feature maps, along with residual connections and

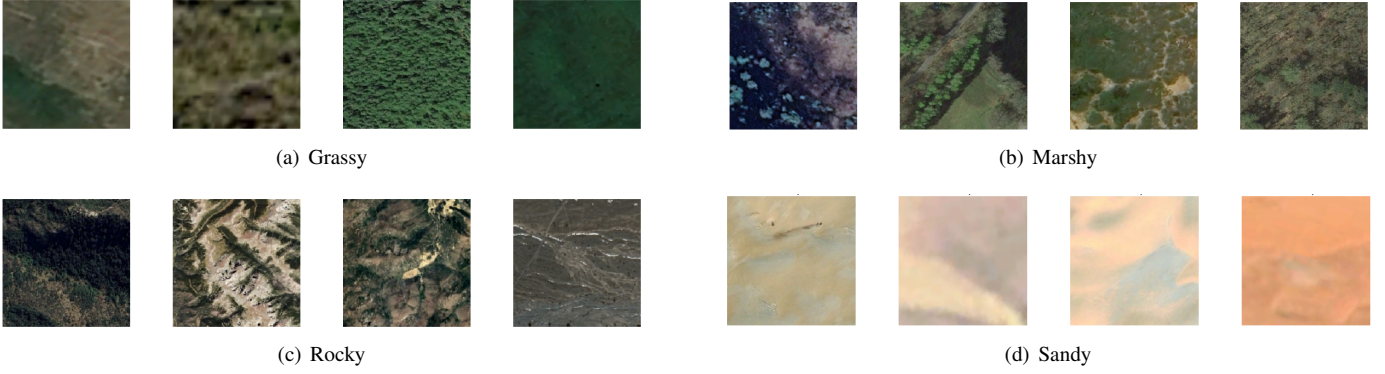


Fig. 3. Terrain Dataset [42]

TABLE I
CLASS DISTRIBUTION

Set	Grassy	Marshy	Rocky	Sandy	Total	Split
Training	8512	7727	7668	7664	31571	70 %
Testing	1824	1657	1644	1644	6769	15 %
Validation	1824	1656	1643	1642	6765	15 %
Total	12160	11040	10955	10950	45105	100 %

layer normalization for improved training speed and performance of the model.

Then, the *GAP* layer is applied to diminish the spatial dimensions of the feature maps by averaging their elements. The vector is then passed through a final layer with a softmax activation function. The softmax function gives the probability distribution of the input image belonging to a particular terrain class.

C. Roughness Extraction Branch

Texture refers to the recurring pattern of localized fluctuations in image intensity. It quantifies how intensities are arranged within a specific region, represented as a feature vector. Statistical approaches prove valuable, especially for analyzing small texture elements, leading to the formation of micro textures.

Image variance quantifies the dispersion of intensity values within an image. It is a dimensionless quantity that indicates how much the intensity values deviate from the mean intensity value.

A high variance signifies that the intensity values are widely distributed across a broad range, which is characteristic of an image with high contrast. A low variance indicates that the intensity values are clustered together, which is characteristic of an image with low contrast.

Variance to be computed from the image histogram is given by:

$$\sigma^2 = \sum_{i=0}^{j-1} (z_i - m)^2 p(z_i) \quad (5)$$

where z_i is the intensity value of the i^{th} pixel, m denotes the mean intensity value & $p(z_i)$ is the probability of the i^{th} pixel having intensity value z_i .

Algorithm 2 Terrain Roughness Extraction

```

1: Input:
   Image:  $I \in \mathbb{R}^{224 \times 224 \times 3}$ 
2: Parameters:
   Patch size:  $P = W \times H$ 
   Variance:  $V = \sigma^2$ 
   Roughness Factor:  $R$ 
   Data Matrix:  $Data_{8 \times 8}$ 
   Step Size:  $s$ 
   Transparency Level :  $\alpha$ 
3: procedure IMPLICITPROPERTIES( $I, s$ )
4:    $P \leftarrow \text{Patchify}(I, P, s)$ 
5:   for  $P \in \text{Patches}$  do
6:      $PatchList \leftarrow PatchList \cup \{P\}$ 
7:      $WindowStride \leftarrow s$ 
8:   end for
9:   for  $V \in \text{Variance}(PatchList)$  do
10:     $Roughness \leftarrow Roughness \cup \{1 - \frac{1}{1+V}\}$ 
11:   end for
12: end procedure
13:  $GlobalRoughness \leftarrow \text{GlobalAverage}(Roughness)$ 
14: procedure VISUALIZE( $GlobalRoughness$ )
15:    $Data \leftarrow \text{CreateMatrix}(GlobalRoughness)$ 
16:    $Data \leftarrow \text{Resize}(Data, W, H)$ 
17:    $Data \leftarrow \text{Normalize}(Data)$ 
18:    $Data \leftarrow \text{ColorMap}(Data)$ 
19:    $O \leftarrow \text{Blend}(I, Data, \alpha)$ 
20:   return  $O$ 
21: end procedure
22: Output:
    $O$ : Terrain image with extracted properties

```

The roughness factor R is a measure of the texture of an image.

$$R = 1 - \frac{1}{1 + \sigma^2} \quad (6)$$

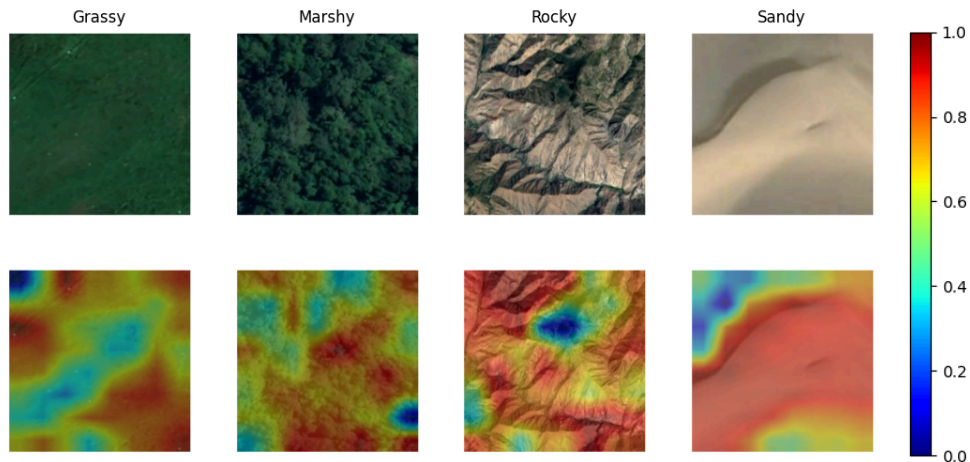


Fig. 4. Roughness Extraction

It is a dimensionless quantity ranging from 0 to 1, where 0 represents a completely smooth image and 1 represents an entirely rough image [16].

Algorithm 2 represents terrain roughness extraction. The input image I is partitioned into patches of size P creating a new collection of patches, PatchList. The process continues by iterating through each patch in PatchList. The variance of each patch is then calculated. The roughness of each patch based on the variance obtained is calculated. Thereafter, a global roughness value is computed by averaging the roughness information stored in the Data Matrix.

A new Data matrix is created to represent the visualized roughness property. The Data matrix is normalized to a common range and resized to match the original image dimensions, and a colormap is applied to the Data matrix to visually represent the roughness levels. Finally, the original image I is combined with the visualized roughness data (Data) using the transparency level to create the final output image O .

IV. RESULTS

This section documents the results obtained after performing different experiments on the remote-sensing dataset consisting of different terrain classes.

A. Dataset and Implementation Detail

The Dataset contains of over 45 thousand images, with more than 10 thousand images for each class i.e. Sandy, Rocky, Grassy, Marshy. The dataset split distribution given in table I. The dataset is available here [42].

In this work, the model is trained using PyTorch on a computer with Intel Core i7-11800H CPU, 16 GB DDR4 RAM, and Nvidia GeForce RTX 3050 Ti GPU for acceleration.

In this study, the Swin transformer network, specifically the Swin-Tiny variant, was employed [14]. The Label Smoothing Cross Entropy loss function was selected for training the network. The AdamW optimizer was utilized for the training process, with 10 epochs configured from training. Additionally, all layers were initialized with learning rate of 0.001.

TABLE II
CLASSIFICATION PERFORMANCE OF DIFFERENT METHODS

Class	MobileNet	ResNet	StrideNET (Ours)
Grassy	95.98	97.69	99.00
Marshy	93.83	98.32	99.00
Rocky	97.89	98.44	99.00
Sandy	94.30	97.03	100.00
Accuracy (%)	95.50	97.87	99.00
F1 score	70.30	93.45	100.00

In the image preprocessing phase, implementation begins by resizing the input image to dimensions of 256x256, followed by cropping to a standardized 224x224 size to ensure consistency across samples. Subsequently, a Swin Transformer architecture is employed for feature extraction, where the embedding dimension is set to 96 to capture rich semantic information.

The model architecture consists of hierarchical processing stages, with varying numbers of transformer layers and attention heads tailored to each level's specific needs. Specifically, a configuration of [2, 2, 6, 2] transformer layers and [3, 6, 12, 24] attention heads across the respective levels are adopted.

To facilitate hierarchical processing, The input image undergoes partitioning into windows, each with a size of 7. This enables the model to effectively capture multi-resolution features for a comprehensive understanding of the input terrain imagery. This thorough approach ensures robust feature representation and discriminative capability, essential for accurate terrain classification tasks.

B. Experimental Results

The classification results are outlined in Table II. The model attains a state of the art classification accuracy of 99% on the remote sensing dataset. It is evident from the results that the proposed StrideNET model surpasses conventional models in terrain recognition tasks. Furthermore, terrain roughness and slipperiness information is determined using a statistical

variance-based texture analysis and is depicted as an overlay on the original image, as illustrated in Fig. 4.

In this study, four types of terrains were considered: Grassy, Marshy, Rocky, and Sandy. The test accuracy achieved for each of these classes exceeds 99%, as demonstrated in Table II.

V. CONCLUSION

In this paper, a novel dual-branch transformer architecture, termed StrideNET, is introduced for the purpose of terrain recognition and roughness extraction. The network comprises of two branches: Terrain recognition branch which uses Swin Transformer that captures long range dependencies in the image, while offering linear computational cost. The Swin Transformer is instrumental in capturing local as well as global features, facilitating the precise identification of four terrain classes, namely grassy, marshy, rocky, and sandy. Roughness extraction branch employs a statistical texture analysis algorithm, for computation of surface properties of roughness and slipperiness. The roughness factor, obtained from variance of histogram of image patches, is used to estimate roughness of the image. Experimental findings showcase that the StrideNET model attains state of the art accuracy, outperforming conventional models.

REFERENCES

- [1] Q. Sang, Y. Zhuang, S. Dong, G. Wang, and H. Chen, "Frf-net: Land cover classification from large-scale vhr optical remote sensing images," *IEEE Geoscience and Remote Sensing Letters*, vol. 17, no. 6, pp. 1057–1061, 2020. DOI: 10.1109/LGRS.2019.2938555.
- [2] K. S. Willis, "Remote sensing change detection for ecological monitoring in united states protected areas," *Biological Conservation*, vol. 182, pp. 233–242, 2015, ISSN: 0006-3207. DOI: <https://doi.org/10.1016/j.biocon.2014.12.006>.
- [3] T. Jucker, J. Caspersen, J. Chave, *et al.*, "Allometric equations for integrating remote sensing imagery into forest monitoring programmes," *Global Change Biology*, vol. 23, no. 1, pp. 177–190, 2017. DOI: <https://doi.org/10.1111/gcb.13388>.
- [4] W. Li and C.-Y. Hsu, "Automated terrain feature identification from remote sensing imagery: A deep learning approach," *International Journal of Geographical Information Science*, vol. 34, no. 4, pp. 637–660, 2020. DOI: 10.1080/13658816.2018.1542697.
- [5] M. A.-A. Hoque, S. Phinn, C. Roelfsema, and I. Childs, "Tropical cyclone disaster management using remote sensing and spatial analysis: A review," *International Journal of Disaster Risk Reduction*, vol. 22, pp. 345–354, 2017, ISSN: 2212-4209. DOI: <https://doi.org/10.1016/j.ijdrr.2017.02.008>.
- [6] J. N. Pelton, S. Madry, and S. Camacho-Lara, *Handbook of Satellite Applications*, 2nd. Springer Publishing Company, Incorporated, 2017, ISBN: 3319233858.
- [7] X. Hu, P. Zhang, and Q. Zhang, "A novel framework of cnn integrated with adaboost for remote sensing scene classification," in *IGARSS 2020 - 2020 IEEE International Geoscience and Remote Sensing Symposium*, 2020, pp. 2643–2646. DOI: 10.1109/IGARSS39084.2020.9324261.
- [8] X. Wang, Y. Zhao, D. Liu, G. Sun, A. Zhang, and J. Li, "A lightweight and multi-scale cnn model for land-cover classification with high-resolution remote sensing images," in *2021 IEEE International Geoscience and Remote Sensing Symposium IGARSS*, 2021, pp. 5989–5992. DOI: 10.1109/IGARSS47720.2021.9553755.
- [9] H. Alhichri, A. S. Alswayed, Y. Bazi, N. Ammour, and N. A. Alajlan, "Classification of remote sensing images using efficientnet-b3 cnn model with attention," *IEEE Access*, vol. 9, pp. 14 078–14 094, 2021. DOI: 10.1109/ACCESS.2021.3051085.
- [10] A. A. Aleissae, A. Kumar, R. M. Anwer, *et al.*, "Transformers in remote sensing: A survey," *Remote Sensing*, vol. 15, no. 7, 2023, ISSN: 2072-4292. DOI: 10.3390/rs15071860.
- [11] M. T. Ribeiro, S. Singh, and C. Guestrin, "'why should i trust you?': Explaining the predictions of any classifier," in *Proceedings of the 22nd ACM SIGKDD International Conference on Knowledge Discovery and Data Mining*, ser. KDD '16, San Francisco, California, USA: Association for Computing Machinery, 2016, pp. 1135–1144, ISBN: 9781450342322. DOI: 10.1145/2939672.2939778.
- [12] A. Dosovitskiy, L. Beyer, A. Kolesnikov, *et al.*, "An image is worth 16x16 words: Transformers for image recognition at scale, 2021. arXiv: 2010.11929 [cs.CV].
- [13] H. Touvron, M. Cord, M. Douze, F. Massa, A. Sablayrolles, and H. Jégou, "Training data-efficient image transformers & distillation through attention, 2021. arXiv: 2012.12877 [cs.CV].
- [14] Z. Liu, Y. Lin, Y. Cao, *et al.*, "Swin transformer: Hierarchical vision transformer using shifted windows," in *2021 IEEE/CVF International Conference on Computer Vision (ICCV)*, 2021, pp. 9992–10 002. DOI: 10.1109/ICCV48922.2021.00986.
- [15] A. Jamali and M. Mahdianpari, "Swin transformer and deep convolutional neural networks for coastal wetland classification using sentinel-1, sentinel-2, and lidar data," *Remote Sensing*, vol. 14, no. 2, 2022, ISSN: 2072-4292. DOI: 10.3390/rs14020359.
- [16] M. K. Bhuyan, *Computer Vision and Image Processing: Fundamentals and Applications*. USA: CRC Press, 2019, pp. 157–158. DOI: <https://doi.org/10.1201/9781351248396>.
- [17] W. Li, B. Zhou, C.-Y. Hsu, Y. Li, and F. Ren, "Recognizing terrain features on terrestrial surface using a deep learning model: An example with crater detection," in *Proceedings of the 1st Workshop on Artificial Intelligence and Deep Learning for Geographic Knowledge Discovery*, ser. GeoAI '17, Association for Computing Machinery, 2017, pp. 33–36. DOI: 10.1145/3149808.3149814.
- [18] W. Li and C.-Y. Hsu, "Automated terrain feature identification from remote sensing imagery: A deep learning approach," *International Journal of Geographical Information Science*, vol. 34, no. 4, pp. 637–660, 2020. DOI: 10.1080/13658816.2018.1542697.
- [19] M. D. Zeiler and R. Fergus, "Visualizing and understanding convolutional networks," in *Computer Vision – ECCV 2014*, Cham: Springer International Publishing, 2014, pp. 818–833.
- [20] S. Xie, R. B. Girshick, P. Dollár, Z. Tu, and K. He, "Aggregated residual transformations for deep neural networks," *2017 IEEE Conference on Computer Vision and Pattern Recognition (CVPR)*, pp. 5987–5995, 2016. DOI: 10.1109/CVPR.2017.634.
- [21] K. Simonyan and A. Zisserman, *Very deep convolutional networks for large-scale image recognition*, 2015. arXiv: 1409.1556 [cs.CV].
- [22] G. Huang, Z. Liu, and K. Q. Weinberger, "Densely connected convolutional networks," *2017 IEEE Conference on Computer Vision and Pattern Recognition (CVPR)*, pp. 2261–2269, 2016. DOI: 10.1109/CVPR.2017.243.
- [23] J. Ahmed and H. Ahmed, "Assessing performance of convolutional features for terrain classification using remote sensing data," in *2019 2nd International Conference on Communication, Computing and Digital systems (C-CODE)*, 2019, pp. 178–183. DOI: 10.1109/C-CODE.2019.8680969.
- [24] S. Basu, S. Ganguly, S. Mukhopadhyay, R. DiBiano, M. Karki, and R. Nemani, "Deepsat: A learning framework for satellite imagery," in *Proceedings of the 23rd SIGSPATIAL International Conference on Advances in Geographic Information Systems*, ser. SIGSPATIAL '15, Seattle, Washington: Association for Computing Machinery, 2015. DOI: 10.1145/2820783.2820816.
- [25] Z. Yu, "Research on remote sensing image terrain classification algorithm based on improved knn," in *2020 IEEE 3rd International Conference on Information Systems and Computer Aided Education (ICISCAE)*, 2020, pp. 569–573. DOI: 10.1109/ICISCAE51034.2020.9236884.
- [26] X. X. Zhu, D. Tuia, L. Mou, *et al.*, "Deep learning in remote sensing: A comprehensive review and list of resources," *IEEE Geoscience and Remote Sensing Magazine*, vol. 5, no. 4, pp. 8–36, 2017. DOI: 10.1109/MGRS.2017.2762307.
- [27] G. Cheng, J. Han, and X. Lu, "Remote sensing image scene classification: Benchmark and state of the art," *Proceedings of the IEEE*, vol. 105, no. 10, pp. 1865–1883, 2017. DOI: 10.1109/JPROC.2017.2675998.
- [28] Y. Yang and S. Newsam, "Bag-of-visual-words and spatial extensions for land-use classification," in *Proceedings of the 18th SIGSPATIAL International Conference on Advances in Geographic Information*

Systems, ser. GIS '10, New York, NY, USA: Association for Computing Machinery, 2010, pp. 270–279. DOI: 10.1145/1869790.1869829.

- [29] A. A. Aleissae, A. Kumar, R. M. Anwer, *et al.*, “Transformers in remote sensing: A survey,” *Remote Sensing*, vol. 15, no. 7, 2023, ISSN: 2072-4292. DOI: 10.3390/rs15071860.
- [30] J. Zhang, H. Zhao, and J. Li, “Trs: Transformers for remote sensing scene classification,” *Remote Sensing*, vol. 13, no. 20, 2021, ISSN: 2072-4292. DOI: 10.3390/rs13204143.
- [31] Y. Bazi, L. Bashmal, M. M. A. Rahhal, R. A. Dayil, and N. A. Ajlan, “Vision transformers for remote sensing image classification,” *Remote Sensing*, vol. 13, no. 3, 2021, ISSN: 2072-4292. DOI: 10.3390/rs13030516.
- [32] L. Bashmal, Y. Bazi, and M. Al Rahhal, “Deep vision transformers for remote sensing scene classification,” Jul. 2021, pp. 2815–2818. DOI: 10.1109/IGARSS47720.2021.9553684.
- [33] M. Bi, M. Wang, Z. Li, and D. Hong, “Vision transformer with contrastive learning for remote sensing image scene classification,” *IEEE Journal of Selected Topics in Applied Earth Observations and Remote Sensing*, vol. 16, pp. 738–749, 2023. DOI: 10.1109/JSTARS.2022.3230835.
- [34] A. Jamali and M. Mahdianpari, “Swin transformer for complex coastal wetland classification using the integration of sentinel-1 and sentinel-2 imagery,” *Water*, vol. 14, no. 2, 2022, ISSN: 2073-4441. DOI: 10.3390/w14020178.
- [35] A. Jamali and M. Mahdianpari, “Swin transformer and deep convolutional neural networks for coastal wetland classification using sentinel-1, sentinel-2, and lidar data,” *Remote Sensing*, vol. 14, no. 2, 2022, ISSN: 2072-4292. DOI: 10.3390/rs14020359.
- [36] V. Suryamurthy, S. Raghavan, A. Laurenzi, N. Tsagarakis, and D. Kanoulas, “Terrain segmentation and roughness estimation using rgb data: Path planning application on the centauro robot,” Sep. 2019. DOI: 10.1109/Humanoids43949.2019.9035009.
- [37] V. Badrinarayanan, A. Kendall, and R. Cipolla, “Segnet: A deep convolutional encoder-decoder architecture for image segmentation,” *IEEE Transactions on Pattern Analysis and Machine Intelligence*, vol. 39, no. 12, pp. 2481–2495, 2017. DOI: 10.1109/TPAMI.2016.2644615.
- [38] E. Romera, J. M. Álvarez, L. M. Bergasa, and R. Arroyo, “Erfnet: Efficient residual factorized convnet for real-time semantic segmentation,” *IEEE Transactions on Intelligent Transportation Systems*, vol. 19, no. 1, pp. 263–272, 2018. DOI: 10.1109/TITS.2017.2750080.
- [39] M. Cordts, M. Omran, S. Ramos, *et al.*, “The cityscapes dataset for semantic urban scene understanding,” in *2016 IEEE Conference on Computer Vision and Pattern Recognition (CVPR)*, 2016, pp. 3213–3223. DOI: 10.1109/CVPR.2016.350.
- [40] I. Laina, C. Rupprecht, V. Belagiannis, F. Tombari, and N. Navab, “Deeper depth prediction with fully convolutional residual networks,” *2016 Fourth International Conference on 3D Vision (3DV)*, pp. 239–248, 2016. DOI: 10.1109/3DV.2016.32.
- [41] Z. Yu, S. Sadati, H. Hauser, P. Childs, and T. Nanayakkara, “A semi-supervised reservoir computing system based on tapered whisker for mobile robot terrain identification and roughness estimation,” *IEEE Robotics and Automation Letters*, vol. 7, pp. 5655–5662, 2022. DOI: 10.1109/LRA.2022.3159859.
- [42] A. Aras. “Terrain recognition.” (2023), [Online]. Available: <https://www.kaggle.com/datasets/atharv1610/terrain-recognition>.